CMS Physics Analysis Summary

Contact: cms-pag-conveners-susy@cern.ch 2011/08/26

Search for supersymmetry in hadronic final states using M_{T2} in 7 TeV pp collisions at the LHC

The CMS Collaboration

Abstract

A search for supersymmetry or similar new physics was carried out using a $\sqrt{s} = 7$ TeV pp collisions data sample corresponding to 1.1 fb^{-1} of integrated luminosity collected by the CMS experiment at the LHC. Fully hadronic final states were selected based on the stransverse mass variable M_{T2}. Two complementary analyses were performed. A first one targets the region of parameter space with medium to high squark and gluino masses, in which the signal can be separated from the Standard Model backgrounds by a strong cut on M_{T2}. A second analysis has been optimized to look for events with a light gluino but heavy squarks. In this case, the M_{T2} cut was relaxed, but higher jet multiplicity and an additional b-tag was required. The dominant backgrounds in both analyses are different. All backgrounds were estimated using both simulation and data-driven methods. As no excess of events over the expected background was observed, exclusion limits were derived.

1 Introduction

This note describes a search for physics beyond the Standard Model in pp collisions collected by the Compact Muon Solenoid (CMS) detector at the Large Hadron Collider (LHC) at a centre-of-mass energy of 7 TeV. The results are based on a data sample collected in 2011, amounting to 1.1 fb^{-1}of integrated luminosity.

It is well known that a search in a hadronic final state accompanied by a large missing transverse momentum ($\not\!\!E_T$) is very sensitive to a broad class of new physics models, including Supersymmetry [1] with R-parity conservation. We present results of a search using the stransverse mass variable, M_{T2} [2, 3], to select new physics candidate events. M_{T2} is the natural extension of the classical transverse mass M_T to the case of supersymmetry where two coloured sparticles are pair-produced and both decay through a cascade of jets and possibly leptons to the Lightest Supersymmetric Particle (LSP). The LSP is not visible in the detector and leads to a missing transverse momentum signature. Though M_{T2} was originally introduced to derive the masses of sparticles involved in the cascade decay, we use it here purely as discovery variable which is found to be very sensitive to the presence of new SUSY-like physics. Indeed, the distribution of M_{T2} reflects the produced particle masses and these are much lighter for the Standard Model background processes than for the SUSY processes we are looking for. Hence, new physics is expected to show up as an excess in the tail of M_{T2}.

The analysis follows two main directions. A first approach, the High M_{T2} analysis, targets events resulting from heavy sparticle production, characterized by large $\not\!\!E_T$ and large M_{T2}. We show with simulation that the remaining Standard Model (SM) backgrounds in the signal region consist of W+jets, $Z \to \nu\bar{\nu}$ and $t\bar{t}$, which are estimated by "data-driven" methods, and apply our selection to the data. This analysis is blind to the case where squarks are heavy and gluinos are light, where the production is dominated by gluino-gluino, the gluinos giving rise to 3-body decays with relatively small $\not\!\!E_T$. As the gluino decay is mediated by virtual squark exchange and the stop and sbottom are expected to be lighter than the first and second generation squarks, these events can be rich in b-quarks. To increase the sensitivity to such processes, a second line of approach, the Low M_{T2} analysis, has been designed in which the minimum of M_{T2} defining the signal region is lowered. To suppress the QCD background, this lowering is compensated by the requirement of at least one b-tagged jet, harder cuts on the jet multiplicity and total energy in the event. We find that this analysis leads to a higher signal to background ratio in the region of heavy squarks and light gluinos and hence improves our sensitivity to this scenario. Finally, some variables are proposed for which the distributions might exhibit a difference between the SM and a SUSY signal, hence providing complementary checks in case of a discovery.

The note is organized as follows: after a brief introduction to M_{T2} and its salient properties in Sect. 2, and a summary of the CMS detector in Sect. 3, we describe in Sect. 4 the data samples used and the event selection. In Sect. 5, the search strategy is presented and applied to the High M_{T2} analysis in Sect. 6 and to the Low M_{T2} analysis in Sect. 7. In these sections the data-driven background estimations are also discussed. As no excess compared to the expectations from SM physics is observed, we proceed with establishing exclusion limits in Sect. 8. In Sect. 9, we study another variable which may also be sensitive to new physics. Finally, Sect. 10 contains our conclusions.

2 Definition of M_{T2} and interpretation

The variable M_{T2} or stranverse mass was introduced [2] to measure the mass of primary pair-produced particles in a situation where both ultimately decay into undetected particles (e.g. neutralino LSPs) leaving the event kinematics underconstrained. It assumes that the two produced sparticles give rise to identical types of decay chains with two visible systems defined by their transverse momenta, $\vec{p}_T^{\,vis(i)}$, energies $E_T^{vis(i)}$, and masses $m^{vis(i)}$. They are accompanied by the unknown LSP transverse momenta, $p_T^{\chi(i)}$. The M_{T2} variable is defined as

$$M_{T2}(m_\chi) = \min_{p_T^{\chi(1)}+p_T^{\chi(2)}=p_T^{miss}} \left[\max\left(m_T^{(1)}, m_T^{(2)}\right)\right], \tag{1}$$

where m_T is the transverse mass of a sparticle decaying to a visible system and its corresponding LSP

$$(m_T^{(i)})^2 = (m^{vis(i)})^2 + m_\chi^2 + 2\left(E_T^{vis(i)} E_T^{\chi(i)} - \vec{p}_T^{\,vis(i)} \cdot \vec{p}_T^{\,\chi(i)}\right) \tag{2}$$

with the LSP mass m_χ remaining as free parameter. A minimization is performed on trial LSP momenta fulfilling the $\not{E}_T$ constraint. For the correct value of m_χ, the distributions of $M_T^{(i)}$ have an endpoint at the value of the primary sparticle mass (similar to the transverse mass distribution for $W \to l\nu$ decay). The largest of the two $M_T^{(i)}$ values can thus be chosen without overshooting the correct sparticle mass. The minimization of $M_T^{(i)}$ then ensures that also the M_{T2} distribution will have an endpoint at the correct sparticle mass. If Initial State Radiation (ISR) can be neglected, an analytic expression for M_{T2} has been computed [4]. In practice, the determination of M_{T2} may be complicated by the presence of ISR or equivalently transverse momentum from upstream decays (UTM) in case M_{T2} is computed for subsystems [4]. In this case, no analytic expression for M_{T2} is known, but it can be computed numerically, see e.g. [5].

In this note, we attempt to use M_{T2} as a variable to distinguish SUSY production events from SM backgrounds. The use of M_{T2} as a discovery variable was first proposed in [6] , but in this note we follow a different approach. Several choices for the visible system used as input to M_{T2} can be considered: purely dijet events (as was the case in [6]), selecting the two leading jets in multijet events or grouping jets together to form two systems or *pseudojets*.

A method to subdivide multijet events in two pseudojets is the reconstruction of "event hemispheres" described in [7], Sect. 13.4. The hemisphere reconstruction works as follows: first, two initial axes (seeds) are chosen. Here, we take them as the directions of the two (massless) jets which have the largest invariant mass. Next, the other jets are associated to one of these axes according to a certain criterion (hemisphere association method). Here, we used the minimal Lund distance, meaning that jet k is associated to the hemisphere with mass m_i rather than m_j if

$$(E_i - p_i cos\theta_{ik})\frac{E_i}{(E_i+E_k)^2} \leq (E_j - p_j cos\theta_{jk})\frac{E_j}{(E_j+E_k)^2}. \tag{3}$$

After all jets are associated to one or the other axis, the axes are recalculated as the sum of the momenta of all jets connected to a hemisphere and the association is iterated using these new axes until no jets switch from one group to the other.

To get a better understanding of the behaviour of M_{T2}, we can take the simple example of M_{T2} without ISR nor upstream transverse momentum. It can be seen from the equation for M_{T2} in

[4] that the whole angular and p_T dependence of M_{T2} is encoded in a variable A_T

$$A_T = E_T^{vis(1)} E_T^{vis(2)} + \vec{p}_T^{\,vis(1)} \cdot \vec{p}_T^{\,vis(2)} \quad (4)$$

and that M_{T2} increases with increasing A_T. Therefore, the minimum value of M_{T2} is reached in configurations where (pseudo)jets are back-to-back and the maximum when they are parallel to each other and with a large p_T. In the simple case where $m_\chi = 0$ is chosen and the visible systems have zero mass, M_{T2} becomes

$$(M_{T2})^2 = 2A_T = 2p_T^{vis(1)} p_T^{vis(2)} (1 + cos\phi_{12}), \quad (5)$$

where ϕ_{12} is the angle between the two (pseudo)jets in the transverse plane. It is seen that this corresponds to the transverse mass of system 1 with an unseen neutral particle of momentum equal to the momentum of system 2 but opposite to it.

SUSY events with large expected $\not\!\!E_T$ and large acoplanarity will be concentrated in the large M_{T2} region. On the contrary, QCD dijet events, being back-to-back, will populate the region of minimum M_{T2}. This will be zero for massless (pseudo)jets if we choose $m_\chi = 0$. Hence, M_{T2} has a built-in protection against QCD jet mis-measurements, even if they have a large $\not\!\!E_T$. However, mismeasured QCD multijet events may give rise to pseudojets away from the back-to-back configuration, leading to $M_{T2} > 0$. For this reason, some protection against $\not\!\!E_T$ from mis-measurements still needs to be introduced. Furthermore, we find that defining pseudo-jets as massless may be a good approach towards further suppressing QCD multijet events in the M_{T2} tail. Other backgrounds consist of events containing true $\not\!\!E_T$, as these can lead to (pseudo)jets away from the back-to-back topology. Candidates are $t\bar{t}$ or W+jets with leptonic decays and $Z(\to \nu\nu)$+jets.

3 CMS detector

The central feature of the CMS apparatus is a superconducting solenoid 13m in length and 6m in diameter which provides an axial magnetic field of 3.8 T. The bore of the solenoid is instrumented with various particle detection systems. The iron return yoke outside the solenoid is in turn instrumented with gas detectors which are used to identify muons. Charged particle trajectories are measured by the silicon pixel and strip tracker, covering $0 < \phi < 2\pi$ in azimuth and $|\eta| < 2.5$, where the pseudorapidity η is defined as $\eta = -\log\ \tan(\theta/2)$, with θ being the polar angle of the trajectory of the particle with respect to the counter-clockwise beam direction. A lead tungstate crystal electromagnetic calorimeter (ECAL) and a brass-scintillator hadronic calorimeter (HCAL) surround the tracking volume and cover the region $|\eta| < 3$. A quartz-steel Cerenkov-radiation-based forward hadron calorimeter extends the coverage to $|\eta| \leq 5$. The detector is nearly hermetic, allowing for energy balance measurements in the plane transverse to the beam directions. A detailed description of the CMS detector can be found elsewhere [8].

4 Data samples, triggers and event selection

The design of the analysis was developed on the basis of Monte Carlo simulation (MC). The MC samples were generated with PYTHIA 6.4.22 [9] and MADGRAPH 5 v1.1 [10], and processed with a detailed simulation of the CMS detector response based on GEANT4 [11]. In order to have sufficient statistics in the tails of the distributions, also two large statistics Z and W + jets samples were produced using a parametrized fast detector simulation of the CMS detector response instead of the GEANT-based simulation. The events were reconstructed and analyzed

in the same way as the data. In case of SM background MC samples we have used the most accurate calculation of the cross sections available in the literature (usually NLO). For the CMS SUSY benchmark signal samples (described in [7] Sect. 13.3 and summarized in Table 1), we used NLO cross sections obtained by weighting the LO cross sections from PYTHIA by sub-process dependent K-factors calculated with Prospino [12].

Table 1: Definition of LM benchmark points, from [7]. For all points, the sign of μ is positive.

Benchmark point	LM1	LM2	LM3	LM4	LM5	LM6	LM7	LM8	LM9
m_0	60	185	330	210	230	85	3000	500	1450
$m_{1/2}$	250	350	240	285	360	400	230	300	175
$\tan\beta$	10	35	20	10	10	10	10	10	10
A_0	0	0	0	0	0	0	0	-300	0

The data used in this analysis were collected by triggers based on the quantity H_T, the scalar sum of transverse momenta of reconstructed and energy corrected calorimeter jets with $p_T \geq$ 40 GeV. These triggers were measured to be nearly 100% efficient in the region where events are selected off-line. In the analysis, events were selected if they had calorimetric $H_T \geq 600$ GeV.

All physics objects used in the analysis are reconstructed in a consistent way using the particle-flow (PF) event description. The particle-flow algorithm [13] identifies and reconstructs individually the particles produced in the collision, namely charged hadrons, photons, neutral hadrons, muons, and electrons. Electrons and muons were considered if they originated from the primary vertex and had $p_T \geq 10$ GeV and $|\eta| \leq 2.4$. Both leptons were required to be isolated, meaning that the transverse momentum sum of charged hadrons, photons, and neutral hadrons surrounding the lepton, with $\Delta R = \sqrt{\Delta\eta^2 + \Delta\phi^2} < 0.3$, divided by the lepton transverse momentum itself was required to be less than 0.2. All non-isolated particles were then clustered into jets by the anti-k_T jet clustering algorithm [14] with a distance parameter $R = 0.5$, to form particle-flow jets [15, 16]. Jet energies are corrected as a function of the transverse momentum and the pseudo-rapidity of the jet, by a factor obtained from the CMS Monte-Carlo simulation. Residual jet energy corrections are applied in the data to bring the jet energy scale to the one observed in the simulation. Jets were required to pass loose quality criteria and have a $p_T \geq 20$ GeV and $|\eta| \leq 2.4$. The missing transverse energy was computed as the absolute value of the vector sum of all the reconstructed particles in the event.

The event preselection required at least one good vertex with a position perpendicular to the beam $\rho < 2$ cm, a position along the beam direction abs(z) < 24 cm and a fit with minimal number of degrees of freedom > 4. Events containing beam background or anomalous calorimeter noise were rejected. At least three good jets were required, the two leading jets with $p_T \geq 100$ GeV.

Several tests were applied to ensure that the selected events were clean and the $\not\!\!E_T$ unbiased. Pile-up was filtered out by using the L1FastJet pile-up subtraction procedure [14] for data and MC. Events were required to be well balanced by imposing a maximum difference between the $\not\!\!E_T$ and $\not\!\!H_T$ vectors of 70 GeV, where the $\not\!\!H_T$ is computed as the vector sum of all selected jets, in order to reject events with an important contribution of soft and/or forward jets to the momentum imbalance. An event was also rejected if there existed hard jets with $p_T \geq 50$ GeV failing the jet identification criteria.

It was argued previously that M_{T2} is protected against jet energy mis-measurements in di-jet events. In multi-jet events such mis-measurement can lead to hemispheres not being back-

to-back any more and hence to larger M_{T2}. To protect against this background, a minimum difference in ϕ between any selected jet and the $\not{E}_T$, $\Delta\phi_{min}(jets, \not{E}_T) \geq 0.3$, was required. Finally, events were vetoed if they contained an identified lepton, to suppress the contributions from $W + jets$, $Z + jets$ and $t\bar{t}$ backgrounds.

5 Search strategy

We will now look at the M_{T2} distributions after having applied all cuts outlined in Section 4. We will separately consider the fully hadronic channels with ≥ 3 jets and a hard M_{T2} cut (the High M_{T2} analysis), mostly sensitive in the region of large squark and gluino masses, and a relaxed M_{T2} cut complemented by a b-tag and higher jet multiplicity (the Low M_{T2} analysis), increasing the sensitivity to the region of low gluino and high squark masses.

Given the event selection outlined above, we do not expect a significant amount of QCD events to enter the signal regions. Nevertheless, we use a data-driven method to estimate an upper limit on the remaining QCD background in the signal regions. For the $W + jets$, $Z + jets$ and $t\bar{t}$ we will demonstrate in the following sections by means of data-driven methods that the data in the control regions are well reproduced by the simulation:

1. A signal region is defined by a lower cut on M_{T2} which optimizes the significance for discovery. Then we define a control region adjacent to the signal region where the QCD background is less than $\sim 1 - 10\%$ of the total background.

2. Data-driven methods are designed for each of the different background contributions. The numbers of events and their relative systematic uncertainties are computed by means of these methods in the control region for both data and MC and in the signal region for the MC only.

3. The predicted numbers of events for all background components in MC and their uncertainties in the control region are summed and compared to the total number of MC events. A validity test is carried out by checking that the total number of MC events agrees with the number of events in data within the uncertainties. This uncertainty is a measure of the accuracy to which the data and the MC prediction are found to agree in the control region.

4. The expectation for the number of background events in the signal region is then taken as the number of data events in the control region multiplied by the ratio, f, of MC events in the signal over MC events in the control region. The statistical uncertainty on the expected background is propagated from the statistical uncertainty on the number of data events in the control region by multiplying with the same factor f. We take into account a systematic error due to the accuracy to which the data-driven and the MC predictions are found to agree: for every background component, the relative systematic uncertainty on the expected background in the signal region is computed as the relative uncertainty on the data-driven prediction using the data in the control region multiplied by the ratio of relative systematic uncertainties on the data-driven predictions using MC events in the signal over the control region. The change in background composition between control and signal region is taken into account. Finally, we also take into account an uncertainty on the ratio f originating from the uncertainties on the parton distribution functions used to predict this ratio.

The results will be systematically compared to the CMS SUSY benchmark points defined in Table 1.

6 High M_{T2} analysis

6.1 Event selection

For this analysis, fully hadronic events with at least 3 jets were selected. Events containing a lepton were vetoed.

Figure 1 shows the M_{T2} distribution based on massless pseudojets reconstructed with the standard hemisphere algorithm, for an integrated luminosity of 1.1 fb^{-1}. For $M_{T2} < 80$ GeV the distribution is completely dominated by QCD events. For medium M_{T2} values, the distribution is dominated by $W + jets$ and $Z \to \nu\bar{\nu}$ events with some contribution from $t\bar{t}$, while in the tail of M_{T2} the contribution from top-quark production becomes negligible and $Z \to \nu\bar{\nu}$ together with $W + jets$ are dominating. We observe an excellent agreement between data and simulation in the core as well as in the tail of the distribution. The white distribution (black dotted line) corresponds to the LM6 signal compared to the MC backgrounds. We see that in presence of a signal, we would expect an excess in the tail of M_{T2}, which is not observed.

In Table 2 we give the corresponding event yields for data and SM MC, after the full selection and for various cuts on M_{T2}.

Table 2: Expected background event yields and observed number of events in data after various M_{T2} cuts for events with ≥ 3 jets. "Other" backgrounds are mostly γ + jets.

Process	QCD	W+jets	Z+jets	Top	Other	Total Bkg.	data
After full selection	322001	869.4	409.2	1090.1	995.8	325365	325365
MT2 $>$ 100 GeV	61.4	162.2	138.7	88.2	2.4	452.9	482
MT2 $>$ 150 GeV	4.0	69.0	75.8	27.7	1.2	177.6	208
MT2 $>$ 200 GeV	0.1	33.7	45.5	9.6	0.8	89.8	105
MT2 $>$ 250 GeV	0.0	17.7	27.7	4.1	0.1	49.6	58
MT2 $>$ 300 GeV	0.0	9.9	19.0	1.2	0.0	30.1	30
MT2 $>$ 350 GeV	0.0	5.8	11.9	0.5	0.0	18.2	17
MT2 $>$ 400 GeV	0.0	3.5	7.3	0.2	0.0	11.0	12
MT2 $>$ 450 GeV	0.0	1.9	4.7	0.2	0.0	6.8	9
MT2 $>$ 500 GeV	0.0	1.2	3.5	0.0	0.0	4.6	7

The column labelled "Other" corresponds mainly to the γ+jets background. The cleaning cuts applied in the selection have a relatively small effect on data and MC compared to the M_{T2} cuts, but they are important to avoid anomalous events in the M_{T2} tail. The lepton veto leaves the QCD background nearly unchanged, while reducing the W+jets and $t\bar{t}$ background by $\sim$ 50% each. It is seen that for all choices of M_{T2} cuts, the observed number of events in data agree within the uncertainties with the SM background expectations from MC.

For the presently collected luminosity, the signal sensitivity is optimized for discovery when choosing the signal region $M_{T2} \geq 400$ GeV or slightly above. From the table, a reasonable definition of the control region is then $200 \leq M_{T2} \leq 400$ GeV.

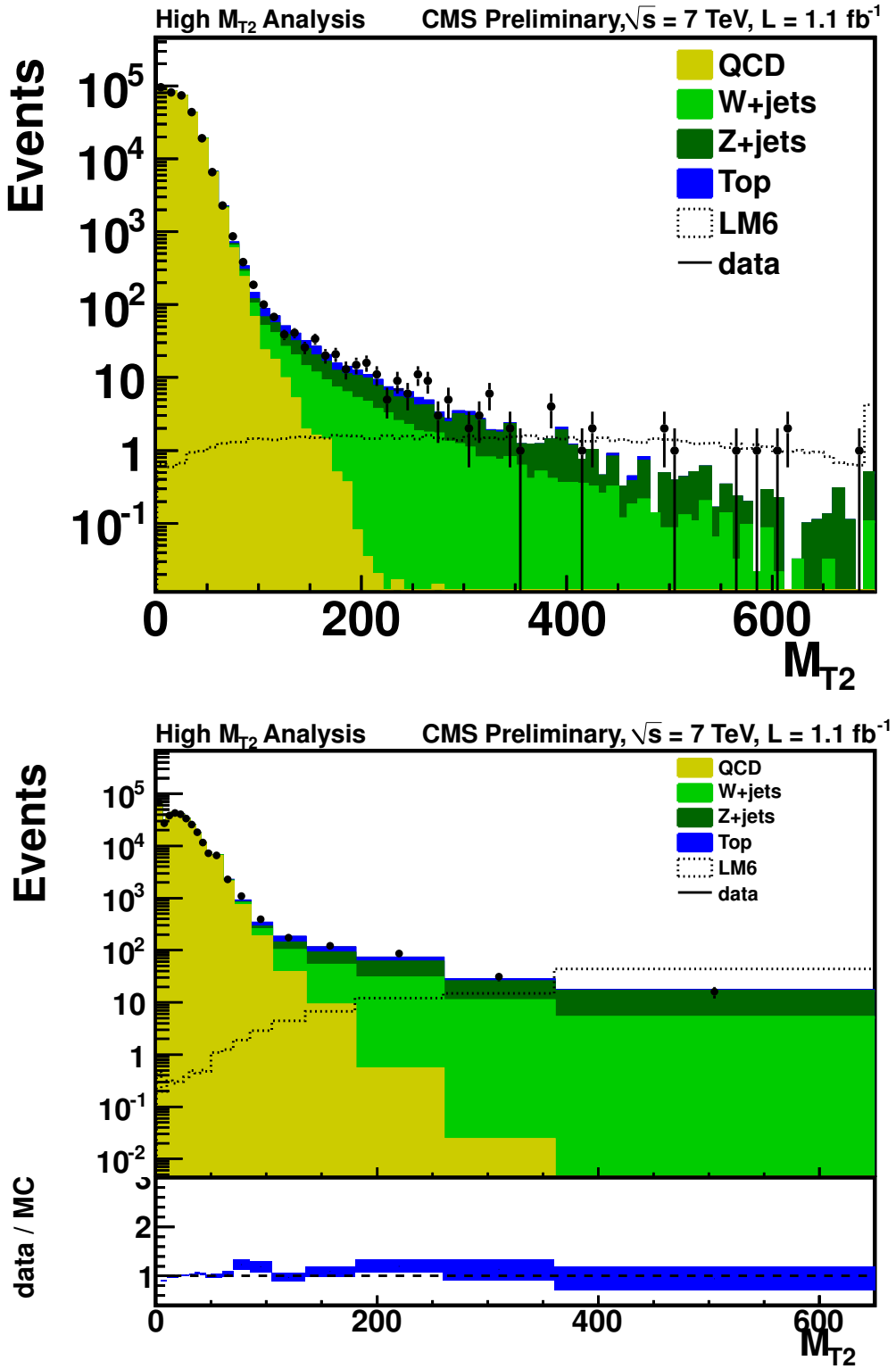

Figure 1: M_{T2} for massless pseudo-jets after having applied all selection cuts, with constant binning (upper) and variable binning (lower). The last bin contains the overflow. The different MC backgrounds are stacked on top of each other and normalized to 1.1 fb^{-1}. The LM6 signal distribution is normalized to the same integrated luminosity and overlayed on the Standard Model backgrounds.

6.2 Data-driven background determination

6.2.1 QCD background

From the simulation, we know that the QCD background is negligible in the tails of the M_{T2} distribution. Nevertheless, it is important to convince ourselves by means of a data-driven method that this is indeed the case.

We have used a data-driven method based on $\Delta\phi_{min}$, the difference in azimuth between the $\not{E}_T$ vector and the closest jet, and M_{T2}. The background in the signal region, defined by $\Delta\phi_{min} \geq 0.3$ and large M_{T2}, is predicted from a control region with $\Delta\phi_{min} \leq 0.2$. The two variables are strongly correlated, but a factorization method can still be applied if the functional form is known for the ratio of numbers of events $r(M_{T2}) = N(\Delta\phi_{min} \geq 0.3)/N(\Delta\phi_{min} \leq 0.2)$ as a function of M_{T2}. It was found in simulation studies, and confirmed in data, that for $M_{T2} > 50$ GeV the ratio falls off exponentially and, therefore, a parameterization of the form

$$r(M_{T2}) = \frac{N(\Delta\phi_{min} \geq 0.3)}{N(\Delta\phi_{min} \leq 0.2)} = exp(a - b \cdot M_{T2}) + c \tag{6}$$

has been used for $M_{T2} > 50$ GeV, where the function is assumed to reach a constant value at large M_{T2} due to extreme tails of the jet energy resolution. From the distribution of QCD simulation events, the fitted parameters are $a = 2.1 \pm 0.4$, $b = (3.6 \pm 0.6)10^{-2}\text{GeV}^{-1}$ and $c = (1.8 \pm 0.6)10^{-3}$. It was checked that the same fit results are obtained when the fit is limited to the region $50 < M_{T2} < 80$ GeV, where the contribution of electroweak processes is still small. The constant term however is only measurable in the signal region and with MC.

First, a validation test was made by estimating the QCD contamination in the signal region using the predicted events in QCD MC in the control region, applying the functional model above. A good agreement was observed. The robustness of the prediction was further checked by varying the fit boundaries and the cut value on $\Delta\phi_{min}$. It was also checked that the presence of a signal, here LM6, does not significantly affect the prediction. Next, the fit is repeated on the data in the region $50 < M_{T2} < 80$ GeV after subtracting the electroweak contribution, leading to the parameter values $a = 1.5 \pm 0.2$, $b = (2.4 \pm 0.3)10^{-2}\text{GeV}^{-1}$. The parameter c is fixed conservatively to the value of the exponential at $M_{T2} = 200$ GeV (below the signal region), where the agreement with data can be tested. The extrapolation of the function to $M_{T2} > 400$ GeV gives the number of background events, 0.2 ± 0.1, but an uncertainty of 100% will conservatively be assumed. This is orders of magnitude larger than the MC prediction, but it still confirms that the QCD contribution is small. Finally, a limit on the constant value of the function at high M_{T2} was derived by considering the extreme case of the jet energy resolution tail, *i.e.* the total loss of a jet. From studying mono- and di-jet events, a conservative upper limit was put on the probability to completely lose a high-p_T jet and it was concluded that the QCD background remains negligible compared to the electroweak backgrounds.

6.2.2 W+jets and $t\bar{t}$ background

The background due to W+jets and semi-leptonic $t\bar{t}$ in the fully hadronic events has the following sources in common:

- leptonic decays of W, where the lepton is unobserved because of the acceptance cuts
- to a lesser extent, leptonic decays of W, where the lepton is within the acceptance, but fails to satisfy the reconstruction, identification or isolation criteria
- decays $W \rightarrow \tau\nu_\tau$ where the τ decays hadronically or to a soft lepton failing the acceptance cuts

These contributions have been estimated as follows. The number of events with lost leptons is estimated from the number where the leptons are found in data and corrected for the probability to lose the lepton. This probability was taken from simulation but an uncertainty was attributed due to the difference between the lepton efficiencies in simulation and in data determined from studies of $Z \rightarrow l^+l^-$-events. This method was applied in the control region where all selection criteria were applied and $200 \leq M_{T2} \leq 400$ GeV. In this region, the QCD background is less than $\sim 1-10\%$ of the total background. First, a successful validation test of the method was made using MC. Then, a prediction was made from the data in the control region and was found to be in agreement with the MC expectation: the estimated number of events with lost muons (electrons) was $7.6 \pm 1.9 \pm 1.5$ ($7.4 \pm 1.8 \pm 1.6$), where the first error is statistical and the second systematic, to be compared with 10.5 (10.5) events in the simulation. The systematic error includes the uncertainty on the lepton efficiencies, acceptance and background subtraction. The total uncertainty represents the accuracy to which the simulation and the data agree in the control region. We proceeded to propagate this uncertainty from the control region to the signal region using the ratio of the systematic uncertainties in simulation, leading to an uncertainty on the lost lepton background prediction in the signal region of 39%.

For the tau contribution, no specific data-driven method was developed. Instead, we verified that both the $W \rightarrow l\nu$ kinematics and hadronic tau decays are well modeled in simulation. First, the agreement between data and MC was checked for all relevant kinematic distributions in a muon control sample with all selection cuts applied, with and without a cut on $H_T > 600$ GeV, and with and without a cut on $M_{T2} > 200$ GeV. All distributions showed satisfactory agreement. We further verified that reweighting the MC muon p_T distribution to the data did not affect the predictions. Hadronic tau decays have been found to be well modeled by the simulation, as is described in [17].

6.2.3 $Z \rightarrow \nu\bar{\nu}$ background

The estimate of the $Z \rightarrow \nu\bar{\nu}$ background was obtained from $W \rightarrow l\nu$ + jets events, where the lepton from the W decay was added to the $\not{E}_T$. Corrections are needed for lepton acceptance, lepton reconstruction efficiency and the ratio between W and Z cross sections (including differences in the shape of distribution on which cuts are applied). Also, the $t\bar{t}$ background to the W+jets events needs to be subtracted, which can be done from data by using b-tagging to identify the top decay and correcting for the b-tagging efficiency. First, a successful validation test was made using MC events in the control region $200 \leq M_{T2} \leq 400$ GeV. Secondly, a prediction was made based on the data in the control region. Lepton efficiencies were taken from studies of $Z \rightarrow l^+l^-$ events in data. The estimated number of $Z \rightarrow \nu\bar{\nu}$ events was $26.3 \pm 6.3 \pm 2.7$, where the first error is statistical and the second systematic, to be compared with 36.5 events in the simulation, showing acceptable agreement. The systematic error includes the uncertainty on the lepton efficiencies, the uncertainty on the b-tagging efficiency from data (used to subtract the $t\bar{t}$ background), the uncertainty on the acceptance from simulation and the uncertainty on the W-to-Z ratio. We then proceeded to propagate this uncertainty from the control region to the signal region using the ratio of the systematic uncertainties in simulation, leading to an uncertainty on the $Z \rightarrow \nu\bar{\nu}$ prediction in the signal region of 38%.

An alternative estimate of the $Z \rightarrow \nu\bar{\nu}$ background was made based on selecting $Z \rightarrow ll$ events in data and adding the leptons to the $\not{E}_T$, but this estimate was suffering from large statistical uncertainties and was therefore not used in the final results.

6.2.4 Background summary

To summarize, the QCD background has a relative uncertainty of 100% for our signal region. The $Z \rightarrow \nu\bar{\nu}$ background estimated from the W + jet events has a total relative systematic uncertainty of 38% in the signal region. The estimate of the W+jets background due to lost leptons results in relative systematic uncertainties on the total W+jets and $t\bar{t}$ of 39% in the signal region.

6.3 Results

In the control region ($200 \leq M_{T2} \leq 400$ GeV), we predict 78.8 events using the MC simulation and we observe 93 events in data. The ratio between the MC events in the signal and control region is 0.136. Therefore, our prediction in the signal region ($M_{T2} \geq 400$ GeV) yields 12.6 events.

After adding the systematic uncertainties from the MC modeling, this becomes

$$Bkgd(M_{T2} \geq 400\text{GeV}) = 12.6 \pm 1.3 \pm 3.5 \text{ events} \quad (7)$$

where the first uncertainty is statistical and the second one the combined systematic error. This is compatible with the 12 events observed in the data.

In Table 3 we give the expected event yield for various SUSY benchmark points after the same selection. The sensitivity to several of the SUSY benchmark points does not decrease dramat-

Table 3: Expected signal event yields after various M_{T2} cuts for events with ≥ 3 jets. The last line gives the efficiency for the signal after cuts at 400 GeV.

Process	LM1	LM2	LM3	LM4	LM5	LM6	LM7	LM8	LM9
After full selection	1208.9	232.2	986.7	672.9	193.9	93.3	51.8	174.9	334.4
MT2 $>$ 100 GeV	958.2	200.3	692.8	518.5	159.0	83.8	27.4	127.2	152.1
MT2 $>$ 150 GeV	802.0	178.5	538.8	429.9	137.9	75.8	16.8	101.4	82.4
MT2 $>$ 200 GeV	647.0	156.7	407.3	347.8	118.4	68.0	10.0	78.7	42.1
MT2 $>$ 250 GeV	502.6	135.0	299.8	275.1	99.6	60.5	5.4	60.3	21.7
MT2 $>$ 300 GeV	371.0	113.2	213.9	212.9	82.7	53.2	3.0	45.2	10.4
MT2 $>$ 350 GeV	254.9	93.1	147.8	156.7	67.0	45.6	1.6	33.8	4.9
MT2 $>$ 400 GeV	163.2	74.3	95.5	109.2	53.0	38.1	0.7	24.5	2.0
MT2 $>$ 450 GeV	86.2	56.4	58.0	71.4	40.5	31.0	0.4	17.2	1.0
MT2 $>$ 500 GeV	40.7	40.2	32.0	43.1	29.5	24.2	0.2	11.5	0.8
Efficiency (400 GeV), %	2.2	8.1	1.7	3.8	7.3	8.3	0.05	2.1	0.02

ically for higher M_{T2} cuts. This may be useful in the future as higher sparticle masses, and hence larger M_{T2} values, will need to be probed.

As can also be observed from Table 3, the signal efficiency is quite high for several of the benchmark points. However, it is very low for points like LM9, showing that the present analysis is not well suited for a search in the region of low $m_{1/2}$ and large m_0. In this region, the $\not{E}_T$ tends to be small and the cuts will need to be optimized differently if we want to have sensitivity to this region. This will be the purpose of the Low M_{T2} analysis, presented in Sect. 7.

An important question is to what extent our background estimate will be affected by the presence of a signal in the control region. If we use for example LM6, the control region would contain 29.9 signal events, compared to the 78.8 background events, i.e. 37% of contamination

which is of the order of the systematic uncertainties. This proportion will, of course, decrease further if we probe higher sparticle masses, as the signal will be spread over a larger range of M_{T2} values. Hence, the contribution of signal events in the control region is not expected to significantly lower the discovery potential. We take into account the effect of signal contamination in calculating the exclusion limits below.

7 Low M_{T2} analysis

7.1 Event selection

It was seen that the High M_{T2} analysis provides a powerful means of searching for SUSY signals, especially in the region of large squark and gluino masses. However, the cuts are too tight for events with heavy squarks and light gluinos, like point LM9. Therefore, somewhat relaxed M_{T2} cuts have been designed to increase the sensitivity to this region. The cut on M_{T2} is reduced to $M_{T2} \geq 150$ GeV. To suppress the increased QCD background, these cuts are compensated by a harder cut $H_T \geq 650$ GeV, the number of jets $N_{jets} \geq 4$ and ≥ 1 b-tag. Also the minimum p_T of the leading jet is required to be at least 150 and the second leading jet 100 GeV. A cut on higher jet multiplicity would have made the search more sensitive to LM9, but is not applied due to potential data/MC discrepancies in the high tail of jet multiplicities.

In Fig.2, the M_{T2} distribution is displayed for events satisfying all Low M_{T2} analysis cuts, using massless pseudo-jets and containing at least one b-tagged jet. The b-tagging is based on the Simple Secondary Vertex (SSV) algorithm [18] where a high purity working point was chosen. This working point has a typical efficiency of approximately 55% for b-jets in our search region (typical transverse momenta of the jets are between 50 and 200 GeV), while the mistagging efficiency for light ($udsg$) jets is of the order of 0.1% and 6-9% for c-jets. The QCD contribution is strongly suppressed in the signal region with $M_{T2} \geq 150$ GeV, and the $t\bar{t}$ contribution dominates over the electroweak ones which are negligible.

The cut flow for data and SM MC is summarized in Table 4. It is seen that for all cuts on M_{T2} the agreement between data and MC is satisfactory.

Table 4: Expected background event yields and observed number of events in data for all relaxed cuts after preselection for events with at least one b-tagged jet.

Process	QCD	W+jets	Z+jets	Top	Other	Total Bkg.	data
After full selection	16857.5	27.8	14.8	445.3	24.6	17370	17370
MT2 $>$ 80 GeV	58.8	7.5	5.5	61.4	0.0	133.3	131
MT2 $>$ 100 GeV	10.1	5.2	4.6	36.9	0.0	56.9	49
MT2 $>$ 120 GeV	3.0	3.6	3.9	23.3	0.0	33.8	26
MT2 $>$ 135 GeV	0.8	2.7	2.6	15.8	0.0	21.9	21
MT2 $>$ 150 GeV	0.2	2.2	1.8	10.8	0.0	15.0	19
MT2 $>$ 165 GeV	0.1	1.7	1.6	7.6	0.0	11.0	12
MT2 $>$ 200 GeV	0.0	0.9	1.2	3.3	0.0	5.4	5
MT2 $>$ 250 GeV	0.0	0.5	0.7	1.5	0.0	2.7	2
MT2 $>$ 300 GeV	0.0	0.3	0.3	0.5	0.0	1.2	0
MT2 $>$ 350 GeV	0.0	0.1	0.1	0.2	0.0	0.4	0

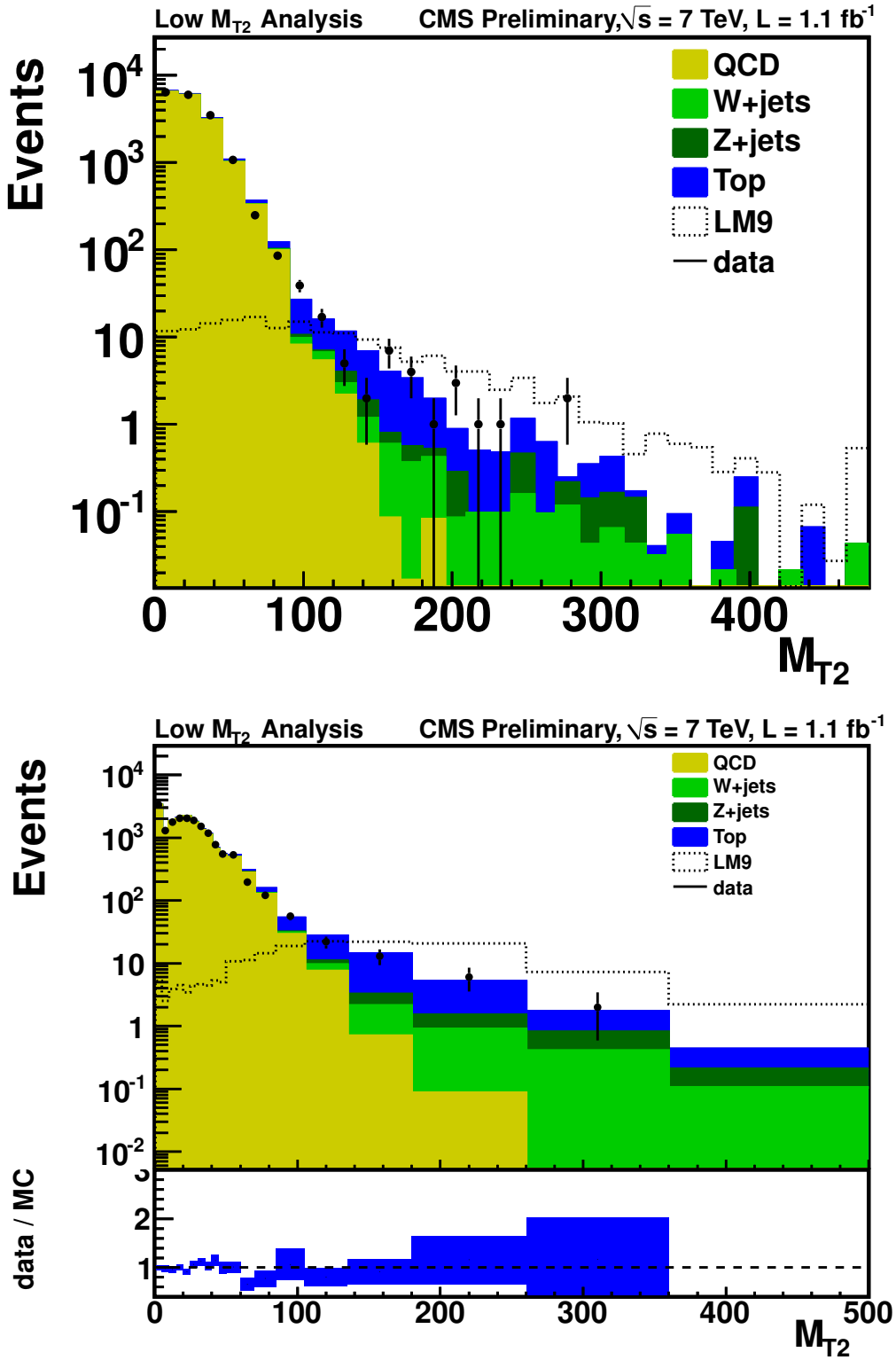

Figure 2: M_{T2} for massless pseudo-jets including at least one b-tagged jet after having applied all Low M_{T2} selection cuts. The upper plot has constant bin size, the lower plot variable bin size. The last bin contains the overflow. The different MC backgrounds are stacked on top of each other and normalized to 1.1 fb^{-1}. The LM9 signal distribution is normalized to the same integrated luminosity and overlayed on the SM backgrounds.

7.2 Data-driven background determination

Although we know from simulation that the QCD background is negligible, a data-driven estimate needs to be made to convince ourselves that it is indeed the case. Unfortunately, the method used for the High M_{T2} analysis cannot be used directly, due to the lack of statistics. Instead, we used the events with all selection cuts applied, except the b-tagging (pre-tagged events). The ratio between the events after b-tagging and the pre-tagged ones as a function of M_{T2} was found compatible with a flat distribution with a ratio of 0.1 ± 0.1. The QCD contribution in the pre-tagged sample was then estimated following the same approach as for the High M_{T2} analysis. The function in equation (6) fitted in the region of 50 to 80 GeV gave a satisfactory representation of the QCD distribution and a validation test performed on the MC was successful. Applied to the data after subtraction of the electroweak and $t\bar{t}$ components results in values $a = 1.4 \pm 0.2$, and $b = (2.3 \pm 0.3) \times 10^{-2}$ for the parameters. From this, the method estimates for $M_{T2} > 150$ GeV a QCD contamination of 7.9 ± 1.2 events, assuming a constant ratio above $M_{T2} > 200$ GeV. Combined with the ratio for b-tagged events above, this yields for the QCD contamination in the low M_{T2} signal region of 0.8 ± 0.8 events, which confirms that the QCD contamination is small.

Given that electroweak processes are small, no data-driven estimate was made for them.

The $t\bar{t}$ background contribution, which dominates, consists in the signal region for $\sim 2/3$ of semi-leptonic decays where the lepton is lost due to the acceptance cuts and for $\sim 1/3$ of hadronic tau decays. Their contribution can be evaluated in the same way as for the High M_{T2} analysis. After all selection cuts are applied, the predicted number of events with electrons in the control region $100 \leq M_{T2} \leq 150$ GeV is $19.9 \pm 6 \pm 4.2$, to be compared to 9 in the MC. For events with muons, the prediction is $6.4 \pm 2.6 \pm 1.7$, compared to 7.6 events in the MC. The uncertainties are dominated by the systematics, which are themselves mainly due to the statistical uncertainties of the efficiencies from the limited MC statistics. The agreement between the estimate from data and the MC is acceptable. Propagating this uncertainty to the signal region leads to a relative uncertainty of 41%.

7.3 Results

For the Low M_{T2} analysis, the signal region is chosen as $M_{T2} \geq 150$ GeV. We find in the control region, defined by $100 \leq M_{T2} \leq 150$ GeV, 41.9 events from the MC against 30 events in data. From Figure 2 we believe to observe a down-fluctuation in data in the control region. The number of MC background events in the signal region amounts to 15.0. After including the systematic uncertainties on the MC modeling, propagated from the individual background contributions, we predict

$$Bkgd(M_{T2} \geq 150\text{GeV}) = 10.6 \pm 1.9 \pm 4.8 \text{ events} \tag{8}$$

The prediction is in moderate agreement with the 19 events observed in data, probably due to a statistical fluctuation in the control region.

The expected event yield for various SUSY benchmark points is shown in Table 5 after the same selection. The signal for some of the benchmark points could again be observable. But more remarkable is the increase in efficiency compared to the High M_{T2} analysis for point LM9, showing that the relaxed M_{T2} cuts indeed increase our sensitivity to the region of heavy squarks and light gluinos.

Table 5: Expected signal event yields after various M_{T2} cuts for events with relaxed cuts and at least one b-tagged jet. The last line gives the efficiency for the signal after the cut $M_{T2} \geq 150$ GeV.

Process	LM1	LM2	LM3	LM4	LM5	LM6	LM7	LM8	LM9
After full selection	147.6	34.4	318.2	117.3	45.7	11.1	17.5	82.0	173.6
MT2 $>$ 80 GeV	120.2	29.9	231.8	91.2	37.2	9.7	10.9	63.2	97.5
MT2 $>$ 100 GeV	112.0	28.6	206.6	83.6	34.7	9.3	9.2	57.5	80.0
MT2 $>$ 120 GeV	103.6	27.0	182.6	76.5	32.0	8.9	7.5	52.4	63.4
MT2 $>$ 150 GeV	91.3	24.7	150.7	65.3	28.4	8.3	5.4	44.6	42.9
MT2 $>$ 200 GeV	70.1	20.6	106.1	49.1	23.0	7.1	3.2	33.2	22.4
MT2 $>$ 250 GeV	49.9	17.2	71.0	36.2	18.2	6.1	1.7	24.5	10.9
MT2 $>$ 300 GeV	34.9	13.4	47.1	25.8	14.2	5.1	0.9	17.5	5.1
MT2 $>$ 350 GeV	21.7	10.5	30.6	17.9	10.7	4.1	0.4	12.2	2.5
Efficiency (150 GeV), %	1.2	2.7	2.8	2.3	3.9	1.8	0.4	3.8	0.4

8 Exclusion limits

The analyses described above showed no excess of event above the SM background expectations. Rather, the data are in agreement with the MC prediction of the SM backgrounds. So, we proceeded to put upper limits on a potential signal. After correcting for efficiencies, when applicable, and taking the systematic uncertainties into account, a 95% upper limit on the number of events has been computed using a CLs formulation [19]. Given the knowledge of the integrated luminosity, assumed to be known with a precision of 4.5%, this limit can be converted into a limit on the cross section times branching ratio within our acceptance.

Based on the numbers of events in Sect. 6 and 7, upper limits at 95% C.L. on the signal cross section times branching ratio within the acceptance are derived using a Gaussian function for the nuisance parameters. Results are summarized in Table 6. It was checked that the limits are

Table 6: Upper limit from the background events on the signal cross section times branching ratio within the acceptance for 1.1 fb^{-1}of integrated luminosity.

Process	$\sigma\times$ BR (pb)	
	observed limit	expected limit
High M_{T2} analysis	0.010	0.011
Low M_{T2} analysis	0.020	0.014

not significantly different when using, instead of a Gaussian function, a Lognormal or Gamma function for the nuisance parameters. These limits may be useful to make simple tests of new models, using the acceptance cuts summarized in Appendix A. For the low M_{T2} analysis, the b-tagging efficiency was taken as part of the acceptance when computing the limit shown in the table. Correcting for the $(52 \pm 6)\%$ b-tagging efficiency would yield an observed (expected) limit of 0.039 (0.025) pb.

Given the observed and MC predicted numbers of events and the 1.1 fb^{-1}of integrated luminosity, Table 7 lists some of the LMx points which are excluded or not. It is seen that the High M_{T2} analysis excludes LM1 to LM6 and LM8 but does not exclude LM7 and LM9. By comparing to Table 5 it is seen that LM8 and LM9 are excluded by the analysis with relaxed M_{T2} cuts. Point LM7 is excluded by none of the analyses, but it is located at $m_0 = 3000$ GeV. It is

Table 7: LMx points excluded (x) or not (-) by our observed upper limits.

Process	LM1	LM2	LM3	LM4	LM5	LM6	LM7	LM8	LM9
High M_{T2} analysis	x	x	x	x	x	x	-	x	-
Low M_{T2} analysis	x	x	x	x	x	-	-	x	x

also important to note that the same point can be excluded simultaneously by several analyses which contain quite different background compositions and hence different systematics.

Exclusion limits at 95% C.L. have been determined in the mSUGRA/CMSSM $(m_0, m_{1/2})$ plane. The results are shown in Fig. 3 for $A_0 = 0$, $\mu > 0$ and $tan\beta = 10$; in Fig. 4 the results from both the High and Low M_{T2} selections are combined by taking the best expected limit in each point (and plotting the corresponding observed limit). The following sources of systematic uncertainties on the signal yield have been considered: the factorization and renormalization scale, the parton density functions, the jet energy scale and the b-tagging efficiency (in the case of the Low M_{T2} analysis). In the case of the High MT2 analysis, the effect of signal contamination in the control region could be significant and has been accounted for.

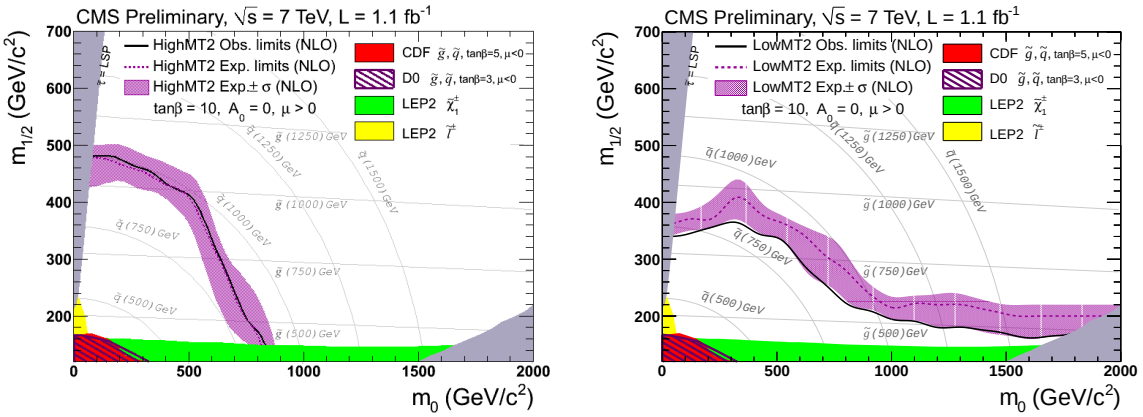

Figure 3: Exclusion limit in the mSUGRA/CMSSM $(m_0, m_{1/2})$ plane for High (left plot) and Low (right plot) M_{T2} selections with $tan\beta = 10$.

It confirms that the High M_{T2} analysis is powerful for a search in the region of high squark and gluino masses, i.e. small m_0 and large $m_{1/2}$, whereas Low M_{T2} analysis extends this sensitivity to large squark and small gluino masses, i.e. large m_0 and small $m_{1/2}$.

9 Additional estimate of the SUSY mass scale using $\sqrt{s}_{min}$

In case an excess is found in the tail of the M_{T2} distribution, it will be important to strengthen the discovery by complementing it with additional variables that reflect the presence of new heavy states. Here we give just one such variable as example.

A variable for measuring the mass scale called $\sqrt{s}_{min}$ was proposed in [20]. It attempts to compute a minimum value for $\sqrt{s}$, the c.m.s. energy of the system. The most interesting aspect of this variable is that it relies only on global event quantities, without requiring the identification of the two decay chains. This variable can be applied to either the total interaction or to a subsystem.

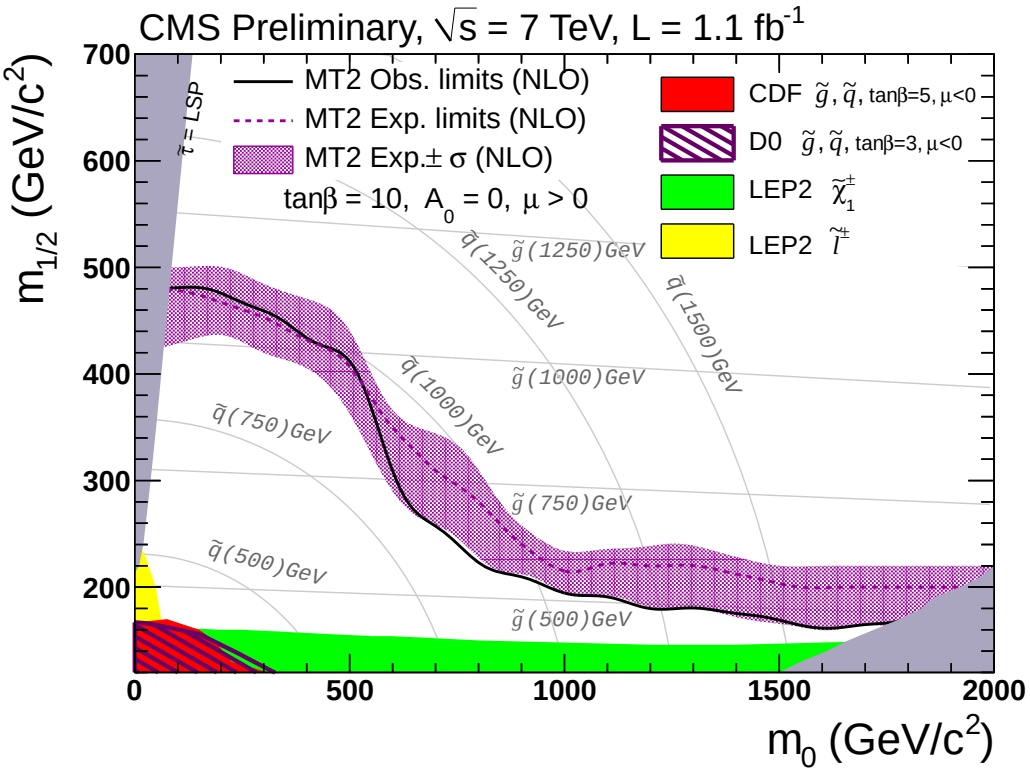

Figure 4: Combined exclusion limit in the mSUGRA/CMSSM $(m_0, m_{1/2})$ plane for the High and Low M_{T2} analyses with $tan\beta = 10$. In each point, the best of the two individual exclusions was taken.

For the overall interaction, in which we are interested here,

$$\sqrt{s}_{min}(M_{miss,min}) = \sqrt{M_{vis}^2 + P_{T,vis}^2} + \sqrt{M_{miss,min}^2 + \not{E}_T{}^2} \tag{9}$$

where M_{vis} and $P_{T,vis}$ refer to the total invariant mass and transverse momentum of all visible particles, $\not{E}_T$ is the missing transverse momentum and $M_{miss,min}$ is the minimum missing mass, i.e. the sum of masses of the unseen particles. As the masses of the unseen particles are a priori unknown, $M_{miss,min}$ remains as a free parameter, often taken to be zero. It was found that if the visible and unseen energies and momenta are measured from all calorimetric towers, the resulting $\sqrt{s}_{min}$ is quite sensitive to ISR and UE [20], [21]. This dependence is largely avoided by using instead reconstruction quantities (e.g. PF jets) and computing the recoil to the measured momenta $\not{H}_T$. The distribution of $\sqrt{s}_{min}$ then displays a peak where the maximum is close to the threshold c.m.s. energy and hence measures $2\times$ the mass of the parent particles.

A distribution of $\sqrt{s}_{min}$ is shown in Fig. 5 for events with ≥ 3 jets satisfying all selection cuts in the signal region with $MT2 \geq 300$ GeV. It illustrates the fact that the LM5 signal would be shifted compared to the background and would strongly enhance it. Moreover, the signal distribution peaks around 1.6 TeV, which corresponds indeed to twice the mass of the produced particles. The same figure displays the $\sqrt{s}_{min}$ distribution for all selected events in data with ≥ 3 jets. Although the statistics is still small, this distribution is in good agreement with the MC expectation and shows no sign of a signal.

Nevertheless, if a signal is observed in the future, a crude estimate of the produced sparticle masses can be obtained from the distribution of $\sqrt{s}_{min}$ for the events in the signal region.

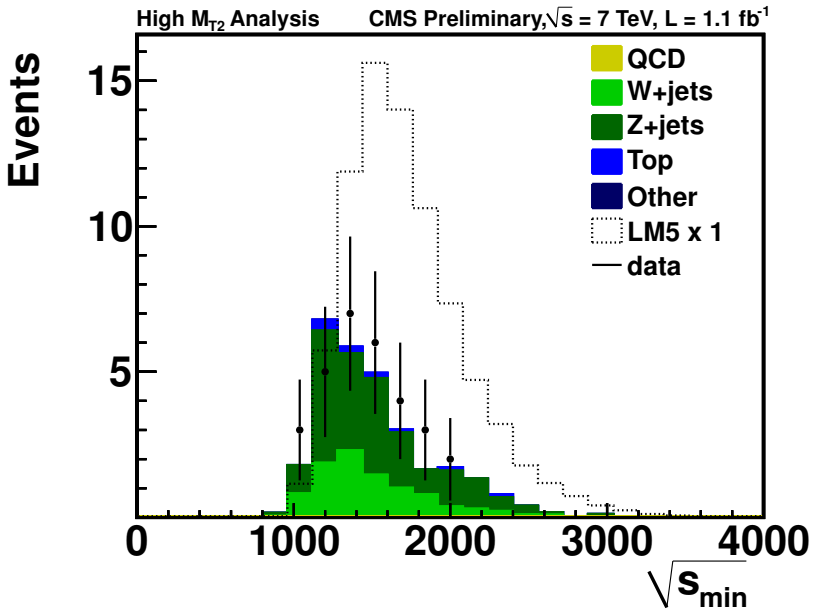

Figure 5: $\sqrt{s}_{min}$ for massless pseudojets including ≥ 3 jets events with $MT2 \geq 300$ GeV.

10 Conclusion

We conducted a search for supersymmetry in hadronic final states using the M_{T2} variable calculated from massless pseudojets. M_{T2} is strongly correlated with $\not{E}_T$ for SUSY processes, yet provides a natural suppression of QCD backgrounds.

A data set containing 1.1 fb^{-1}of integrated luminosity in $\sqrt{s} = 7$ TeV pp collisions taken with the CMS detector during the 2011 LHC run was analyzed. All candidate events were selected using hadronic triggers. Two complementary analyses were performed. The High M_{T2} analysis, targets events from moderately heavy squarks and gluinos which feature naturally a sizeable $\not{E}_T$. The analysis was based on multi-jet events with ≥ 3 jets and events containing a lepton were vetoed to suppress electroweak processes and $t\bar{t}$ production. The SM background prediction from the MC was supplemented by a data-driven estimation, confirming that the MC gives a realistic estimate. We have shown that the tail of the M_{T2} distribution, obtained after this selection, is very sensitive to a potential SUSY signal. No excess beyond the Standard Model expectations has been found; the agreement between the data and the Standard Model predictions is very good. A second line of approach, the Low M_{T2} analysis, was designed to increase the sensitivity to events with heavy squarks and light gluinos, in which the $\not{E}_T$ tends to be smaller. Therefore, the cut on M_{T2} was relaxed and compensated by requesting at least one b-tagged jet and a larger jet multiplicity to suppress the QCD background. A good agreement between the SM background and the data was again observed. It was confirmed that a higher signal to background ratio in the region of heavy squarks and light gluinos is found, which extends the sensitivity to this scenario, compared to the first line of approach.

As no evidence for a signal was found, we set upper limits on the cross section times branching ratio within our acceptance. Also, exclusions limits were established in the mSUGRA/CMSSM parameter space.

A Testing other models

The upper limits on the cross section times branching ratio within our acceptance can be used to verify the compatibility of other models with our results.

An accurate test of the compatibility of another model would require the detailed simulation of this model in the CMS detector. But if we assume that the efficiencies for the SM background and for the model are not too different, the test can be significantly simplified. For this reason, efficiency corrected numbers of events and cross sections are presented in Table 6, so that only the acceptance cuts need to be taken into account. This may be sufficient to test the validity of a model to a reasonable approximation. To help making such a check, we briefly recall the cuts defining our acceptance:

- veto events with electrons or muons with $p_T > 10$ GeV, $|\eta| < 2.4$
- at least 3 jets with $p_T > 20$ GeV, $|\eta| < 2.4$
- the leading jet and second leading jet $p_T >$ 100 GeV
- $\not\!\!E_T$ $>$ 30 GeV
- $\Delta\phi(jet, MET) \geq 0.3$

In addition, for the High M_{T2} analysis cuts:

- $H_T \geq 600$ GeV
- $M_{T2} \geq 400$ GeV

and for the Low M_{T2} analysis cuts:

- number of jets ≥ 4
- the leading jet $p_T >$ 150 GeV
- $H_T \geq 650$ GeV
- at least 1 b-jet
- $M_{T2} \geq 150$ GeV

For the low M_{T2} analysis, the b-tagging efficiency in the search region was $(52 \pm 6)\%$.

References

[1] S. P. Martin, "A Supersymmetry Primer", arXiv:hep-ph/9709356.

[2] C. G. Lester and D. J. Summers, "Measuring masses of semi-invisibly decaying particles pair produced at hadron colliders", *Phys. Lett.* **B463** (1999) 99–103, arXiv:hep-ph/9906349. doi:10.1016/S0370-2693(99)00945-4.

[3] A. Barr, C. Lester, and P. Stephens, "m(T2) : The Truth behind the glamour", *J. Phys.* **G29** (2003) 2343–2363, arXiv:hep-ph/0304226. doi:10.1088/0954-3899/29/10/304.

[4] M. Burns, K. Kong, K. T. Matchev et al., "Using Subsystem MT2 for Complete Mass Determinations in Decay Chains with Missing Energy at Hadron Colliders", *JHEP* **03** (2009) 143, arXiv:0810.5576. doi:10.1088/1126-6708/2009/03/143.

[5] H.-C. Cheng and Z. Han, "Minimal Kinematic Constraints and MT2", *JHEP* **12** (2008) 063, arXiv:0810.5178. doi:10.1088/1126-6708/2008/12/063.

[6] A. J. Barr and C. Gwenlan, "The race for supersymmetry: using mT2 for discovery", *Phys. Rev.* **D80** (2009) 074007, arXiv:0907.2713. doi:10.1103/PhysRevD.80.074007.

[7] CMS Collaboration, "CMS technical design report, volume II: Physics performance", *J. Phys. G* **34** (2007) 995–1579. doi:10.1088/0954-3899/34/6/S01.

[8] CMS Collaboration, "The CMS experiment at the CERN LHC", *JINST* **3** (2008) S08004. doi:10.1088/1748-0221/3/08/S08004.

[9] T. Sjostrand, S. Mrenna, and P. Z. Skands, "PYTHIA 6.4 Physics and Manual", *JHEP* **05** (2006) 026, arXiv:hep-ph/0603175. doi:10.1088/1126-6708/2006/05/026.

[10] J. Alwall, M. Herquet, F. Maltoni et al., "MadGraph 5 : Going Beyond", *JHEP* **1106** (2011) 128, arXiv:1106.0522. * Temporary entry *. doi:10.1007/JHEP06(2011)128.

[11] GEANT4 Collaboration, "GEANT4: A simulation toolkit", *Nucl. Instrum. Meth.* **A506** (2003) 250–303. doi:10.1016/S0168-9002(03)01368-8.

[12] W. Beenakker, R. Hopker, and M. Spira, "PROSPINO: A program for the PROduction of Supersymmetric Particles In Next-to-leading Order QCD", arXiv:hep-ph/9611232.

[13] CMS Collaboration, "Particle Flow Event Reconstruction in CMS and Performance for Jets, Taus and MET", *CMS Physics Analysis Summary* **CMS-PAS-PFT-09-001** (2009).

[14] M. Cacciari, G. P. Salam, and G. Soyez, "The anti-k_t jet clustering algorithm", *JHEP* **04** (2008) 063, arXiv:0802.1189. doi:10.1088/1126-6708/2008/04/063.

[15] CMS Collaboration, "Jet Performance in pp Collisions at sqrts=7 TeV", *CMS Physics Analysis Summary* **CMS-PAS-JME-10-003** (2010).

[16] CMS Collaboration, "Commissioning of the Particle-Flow reconstruction in Minimum-Bias and Jet events at sqrts=7 TeV", *CMS Physics Analysis Summary* **CMS-PAS-PFT-10-002** (2010).

[17] CMS Collaboration, "Tau Identification in CMS", *CMS-PAS-TAU-11-001* (2011).

[18] CMS Collaboration, "Commissioning of b-jet identification with pp Collisions at $\sqrt{s}$=7 TeV", *CMS Physics Analysis Summary* **CMS-PAS-BTV-10-001** (2010).

[19] Particle Data Group Collaboration, "Review of particle physics", *J. Phys.* **G37** (2010) 075021. doi:10.1088/0954-3899/37/7A/075021.

[20] P. Konar, K. Kong, K. T. Matchev et al., "RECO level $\sqrt{s}_{min}$ and subsystem $\sqrt{s}_{min}$", *JHEP* **06** (2011) 041, arXiv:1006.0653. doi:10.1007/JHEP06(2011)041.

[21] A. Papaefstathiou and B. Webber, "Effects of invisible particle emission on global inclusive variables at hadron colliders", *JHEP* **1007** (2010) 018, arXiv:1004.4762. doi:10.1007/JHEP07(2010)018.